A TRANSIENT, AXISYMMETRIC FORMULATION FOR MODELING OF COMPOSITE MATERIALS

Min Eig Lee and Nathan Ida

Department of Electrical Engineering
University of Akron
Akron, Ohio, 44325

INTRODUCTION

The electrically small loop is of great practical importance in finding direction and probing magnetic fields. In [1], it was proposed for communication from above ground to observation points within coal mines. In this paper, the interactions of electromagnetic field, produced by a current-excited small loop, with lossy and lossless materials are investigated. The use of a small loop for the NDE of composite materials is also presented. To achieve these goals, solutions of interface problems become necessary. Since the exciting current is not restricted to be time-harmonic, we will solve the problems in the time domain. Also, to obtain economic requirements for computer resources, both storage and running time, a potential approach instead of vector field codes is developed.

The solution procedures start from defining the field variables in terms of a vector potential. This potential function is used to model the problem in the time domain. The finite-difference time-domain (FD-TD) techniques are employed to discretize the problem both in time and in space. Numerical results, both transient and sinusoidal steady state, are first validated by the image method. Finally, the solution of a small loop placed over a composite sheet is presented and discussed. This paper concentrates on high frequency applications.

FORMULATION OF THE PROBLEMS

A typical geometry is that of a small loop antenna placed horizontally over a half space of lossy material. The Maxwell's equations required are:

$$\nabla \cdot \mathbf{D} = q \,, \tag{1}$$

$$\nabla \times \mathbf{E} = -\frac{\partial \mathbf{B}}{\partial t} \,, \tag{2}$$

$$\nabla \times \mathbf{H} = \mathbf{J} + \frac{\partial \mathbf{D}}{\partial t} \,, \tag{3}$$

$$\nabla \cdot \mathbf{B} = 0 \,, \tag{4}$$

where $\mathbf{D}$ is the electric flux density, $\mathbf{E}$ is the electric field intensity, $\mathbf{B}$ is the magnetic flux density, $\mathbf{H}$ is the magnetic field intensity, q is the electric charge density, and $\mathbf{J}$ is the current density. Using Lorenz's gauge, the scalar potential V and the vector potential $\mathbf{A}$ are defined in the following way:

$$\mathbf{B} = \nabla \times \mathbf{A}, \qquad \nabla \cdot \mathbf{A} = -\mu\sigma V - \mu\epsilon \frac{\partial V}{\partial t} \,, \tag{5}$$

Review of Progress in Quantitative Nondestructive Evaluation, Vol. 9
Edited by D.O. Thompson and D.E. Chimenti
Plenum Press, New York, 1990

$$\mathbf{E} = -\nabla V - \frac{\partial \mathbf{A}}{\partial t} , \tag{6}$$

In terms of these two potentials, the governing equations are:

$$\nabla^2 V = \mu\sigma\frac{\partial V}{\partial t} + \mu\epsilon\frac{\partial^2 V}{\partial t^2} - \frac{q}{\epsilon} , \tag{7}$$

$$\nabla^2 \mathbf{A} = \mu\sigma\frac{\partial \mathbf{A}}{\partial t} + \mu\epsilon\frac{\partial^2 \mathbf{A}}{\partial t^2} - \mu\mathbf{J}_s . \tag{8}$$

Here, $\mathbf{J}_s$ is the source current. The consideration here is to assume that the loop is very small, so that the current distribution in the loop is uniform. This creates a three-dimensional axisymmetric situation. The cylindrical coordinates are then assigned to the space in such a way that the axis of the loop is in the z direction, and the current is in the ϕ direction. Since the current is in the ϕ direction, the magnetic vector potential $\mathbf{A}$ and the electric field $\mathbf{E}$ have only a ϕ component, i. e., $\mathbf{A} = A\phi$ and $\mathbf{E} = E\phi$. Since the current is uniform in the ϕ direction, the ϕ variations of $\mathbf{A}$, $\mathbf{E}$, and V are all zero. Thus, from (6), $E = -\partial A/\partial t$. As a result, both $\mathbf{H}$ and $\mathbf{E}$ can be obtained from the ϕ component of the magnetic vector potential A. Therefore, the whole problem can be modeled with this potential function A as follows. The governing equations are:

$$\frac{\partial^2 A}{\partial z^2} + \frac{\partial^2 A}{\partial \rho^2} + \frac{1}{\rho}\frac{\partial A}{\partial \rho} - \frac{A}{\rho^2} = \mu_a\epsilon_a\frac{\partial^2 A}{\partial t^2} \qquad \textit{in air, excluding the source,} \tag{9}$$

$$\frac{\partial^2 A}{\partial z^2} + \frac{\partial^2 A}{\partial \rho^2} + \frac{1}{\rho}\frac{\partial A}{\partial \rho} - \frac{A}{\rho^2} = \mu_m\sigma_m\frac{\partial A}{\partial t} + \mu_m\epsilon_m\frac{\partial^2 A}{\partial t^2} \qquad \textit{in lossy medium.} \tag{10}$$

The interface conditions come from the continuities of tangential electric and magnetic field intensities across the interface. The former leads to: $\partial A^-/\partial t = \partial A^+/\partial t$, where the minus sign represents the potential in air, and the plus sign represents that in the lossy medium. The latter leads to: $\mu_r\partial A^-/\partial z = \partial A^+/\partial z$, where μ_r is the relative permeability of the conducting medium. The loop current is assumed to be switched on at $t = 0$. With a retarded time for potential to arrive at the interface, the potentials A^- and A^+ on the interface are all zero at $t = 0$. Therefore, the first interface condition leads to: $A^- = A^+$. Initial conditions are: $A(\rho, z, 0) = A_i(\rho, z, 0)$ and $(\partial A/\partial t)(\rho, z, 0) = (\partial A_i/\partial t)(\rho, z, 0)$, where A_i is the incident potential. Different radiation boundary conditions are needed in different media. In free space, the following condition is used on a far-field boundary:

$$\frac{\partial A_o}{\partial r} + \mu_a\epsilon_a\frac{\partial A_o}{\partial t} + \frac{1}{r}A_o = 0 , \tag{11}$$

where A_o is the outgoing component of A. In lossy dielectrics, based on [2], the following boundary condition is obtained:

$$\frac{\partial A_o}{\partial r} + \mu_m\epsilon_m\frac{\partial A_o}{\partial t} + \left(\frac{\sigma_m}{2}\sqrt{\frac{\mu_m}{\epsilon_m}} + \frac{1}{r}\right)A_o = 0 . \tag{12}$$

In good conductors, the boundary condition is simply $A_o = 0$.

NUMERICAL METHODS

The problem considered here has a source in the solution domain. The source gives the incident field component. The treatment here is to model the source by the incident components at a group of grid points, which are near to and enclose the source. For time-harmonic fields, define $\overline{A}$ to be the complex phasor of A, i. e., $Re(\overline{A}) = A$. The incident magnetic vector potential produced by a small loop, carrying a spatially uniform current I under time-harmonic excitation, is [3]:

$$\overline{A_i} \longrightarrow \frac{I\pi a^2}{4\pi}e^{i(k_a r' - \omega t)}\left(\frac{ik_a}{r'} + \frac{1}{(r')^2}\right)\sin\theta , \tag{13}$$

where a is the radius of the loop, r' is the distance of the observation point from the loop's center, ω is the angular velocity of the exciting current and θ is the angle which the position vector r' makes with the z-axis. For the points on the axis, $\theta = 0$. Thus, the incident components of A at these points are zero. Also by axial symmetry, it is easily verified that the scattered components of A at these points cancel each other. Therefore, the condition $A = 0$ is imposed on the axis and the singularity is avoided.

The FD-TD techniques are used to discretize the problem both in space and in time. Due to an axial symmetry, only the potentials in the right-half plane need be calculated. The forward-backward difference scheme in [4] is used to implement the radiation boundary conditions. In the present situations, both the incident field and the scattered field are outgoing. Therefore, the radiation conditions are used to take care of the total field. Numerical implementation of the interface conditions is similar to that in [4].

NUMERICAL EXPERIMENTS

For the following experiments, the source is switched on at $t = 0$.

Experiment I

This numerical experiment is intended to validate the numerical methods described above. The geometry is that of a small loop antenna, which produces a sinusoidal incident wave at 1 GHz, placed over a sheet of aluminum. The loop's radius is assumed to be 0.7995443 mm. The loop's plane is assumed to be 0.9994304 mm above the interface boundary, which is on the plane $z = 0$. The mesh size and useful parameters are shown in Fig. 1. The numerical methods described above were implemented in a computer program running on a SUN4/260 workstation. The space separation Δz is 6.24644×10^{-3}m. The time interval Δt is chosen to be 1.473306×10^{-11} second. The numerical solution was obtained after 2715 time steps, i. e., 40 periods from the beginning. The CPU time is 2.33 minutes. From the history plot at a point P(40,40), the solution is found to be at a sinusoidal steady state. The contour plot of the numerical results is plotted in Fig. 2.

The analytic solution is obtained through the image method. The percentage root mean square error in the computational domain with vertices (j1,k1), (j2,k1), (j2,k2), and (j1,k2) is defined in the following way:

$$e_{rms} = \frac{\sqrt{\frac{\sum_{j=j1}^{j2}\sum_{k=k1}^{k2}(A_a - A_n)^2}{N}}}{\sqrt{\frac{\sum_{j=j1}^{j2}\sum_{k1}^{k2}(A_a)^2}{N}}}, \tag{14}$$

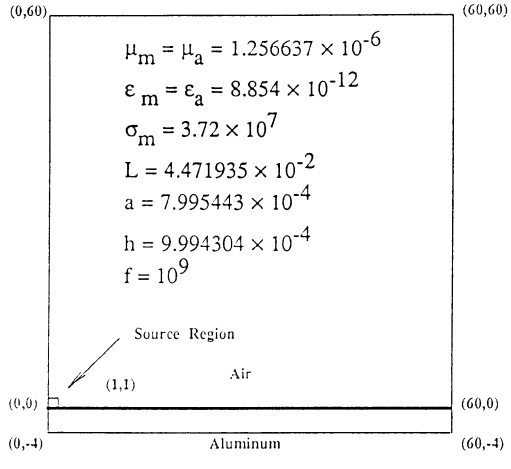

Figure 1. Grid size and important parameters for experiment I.

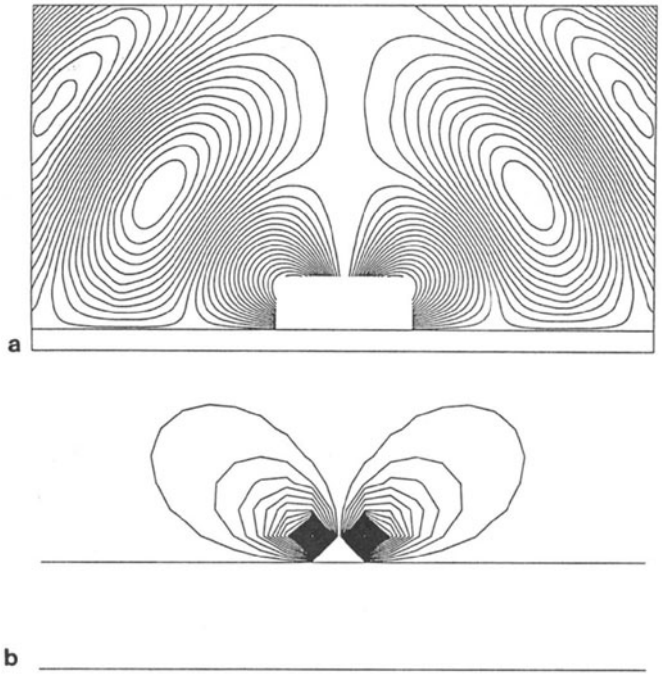

Figure 2. Contour plot of the numerical solution in experiment I: (a)A region of 40 cm by 75 cm excluding the central area. (b)The central area.

where A_a is the analytic solution, A_n is the numerical solution, and $N = (j2 - j1 + 1)(k2 - k1 + 1)$. Using this definition, e_{rms} in the whole computational domain was calculated to be 10.40%. For the domain with vertices (20,20), (40,20), (40,40), and (20,40), e_{rms} was 4.15%. For the domain with vertices (20,20), (60,20), (60,60), and (20,60), e_{rms} was 5.30%. From these results, it is clear that the major error occurs near the source. This is due to the fact that A changes rapidly with the distance away from the source's center in this region. A minor error occurs near the artificial boundary because of the nonphysical reflection from the radiation boundary.

To reduce the major error, the grid spacing must be refined, especially near the source. In the second calculation, the grid spacing is refined to half the previous value. The physical situations are kept unchanged. Note that the grid point (2j,2k) in the current coordinates corresponds to the grid point (j,k) in the previous coordinates. The numerical solution obtained is compared to the previous analytic solution. e_{rms} in the whole computational domain was found to decrease to 4.75%. In this way, the numerical solution was greatly improved.

To reduce the error from the nonphysical reflection, the radiation boundary must be moved farther away from the source. In the third calculation, the geometry and grid spacing are kept the same except that the artificial boundary is moved to twice the distance away from the source. Compared to the previous analytic solution, e_{rms} in the region with vertices (0,-4), (60,-4), (60,60), and (0,60) was found to be 10.36%. For the region with vertices (20,20), (60,20), (60,60), and (20,60), e_{rms} is 4.34%. In this way, the nonphysical reflection from the artificial boundary has been reduced.

Experiment II

In this experiment, the small loop of the previous experiment is excited by a current with a Gaussian time variation, i. e. , $I = I_0 exp(-k_g^2(t-t_0)^2)$, where k_g is a constant defining the bandwidth and t_0 is the time instant when the pulse peak occurs. The incident magnetic vector potential, produced by this current, is calculated from:

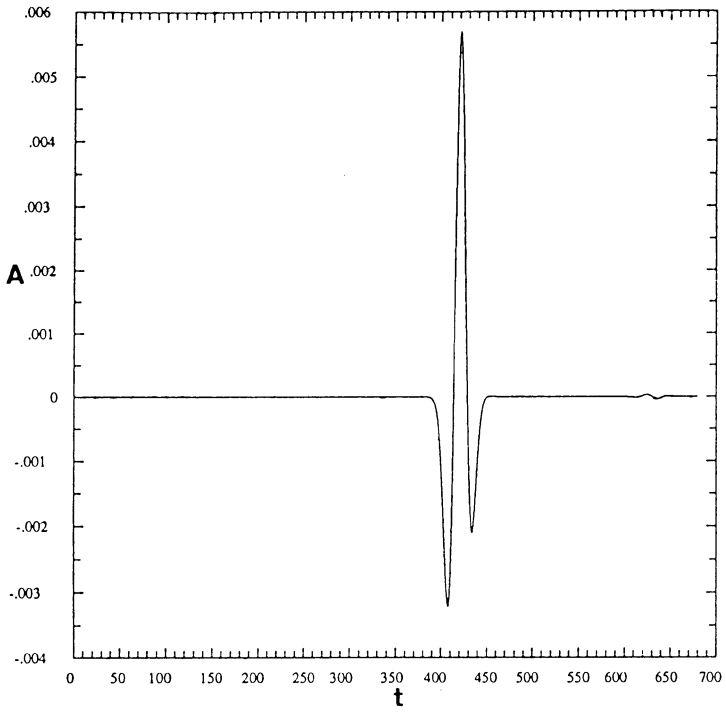

Figure 3. History plot at P(40,40) in experiment II, numerical solution. The unit used on the horizontal axis is 14.73 ps.

$$A_i \rightarrow \frac{I_0 a^2}{4} e^{-k_g^2(k_a r' - t + t_0)^2} \left(\frac{2k_g^2 \cdot k_a(k_a r' - t + t_0)}{r'} + \frac{1}{(r')^2} \right) \sin\theta \ , \tag{15}$$

where $k_a = \sqrt{\mu_a \epsilon_a}$. Details of derivation of this formula, in scaled form, can be found in [5]. To reduce the error from the nonphysical reflection, the artificial boundary is moved to twice the distance away from the source. The history plot at point P(40,40) is shown in Fig. 3. The analytic solution is obtained from the image method and is plotted in Fig. 4. When the two plots are compared to each other, an excellent agreement is found and the numerical methods can be justified.

Experiment III

In this experiment, the sheet of aluminum in experiment I is replaced by a sheet of composite material. To simulate the practical situation, the thickness of the composite material is assumed to be 12.5 mm. The electric and magnetic properties of the composite material are assumed to be: $\epsilon_r = 3$, $\sigma = 10^{-10}$, and $\mu = \mu_a$. The mesh size and useful parameters are shown in Fig. 5. The contour plot at a sinusoidal steady state is shown in Fig. 6. The contour plot without the composite material is shown in Fig. 7. It is found that the presence of the composite material tends to modify the field distribution near the interface. When the permittivity of the composite material becomes larger, see Fig. 8 for $\epsilon_r = 6$, the modification is more remarkable. This phenomenon is suggested for the NDE of composite materials, during either the processing or maintainence period.

CONCLUSIONS

A transient, axisymmetric numerical model for electromagnetic interface problems has been derived. The formulas are validated by numerical experiments, both in transient and sinusoidal steady-state situations. Also, the numerical model has been applied to the practical NDE of composite materials.

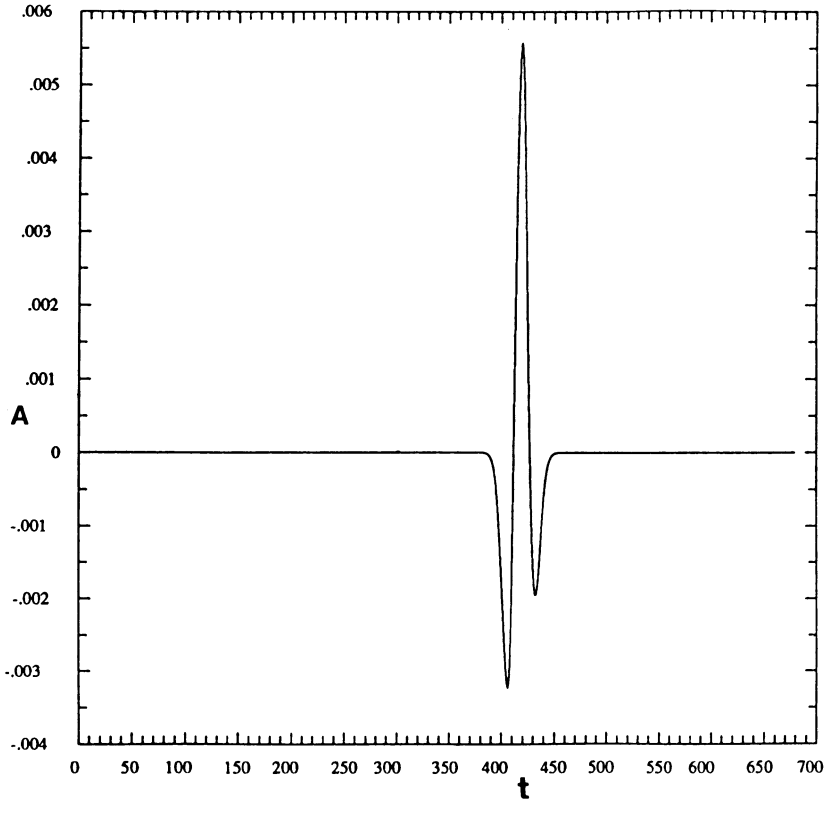

Figure 4. History plot at P(40,40) in experiment II, analytic solution. The unit used on the horizontal axis is 14.73 ps.

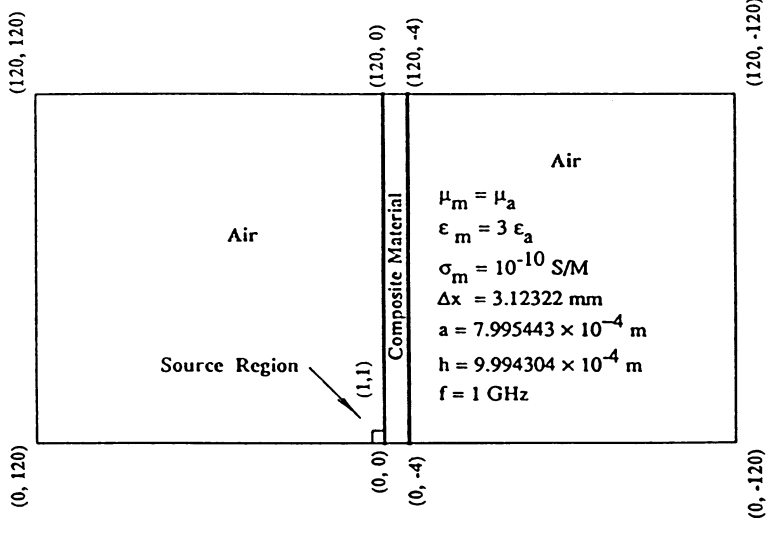

Figure 5. Grid size and important parameters for experiment III.

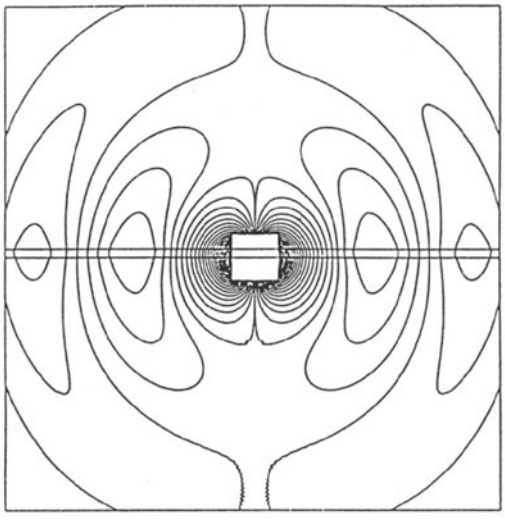

Figure 6. Contour plot in experiment III, $\epsilon_r = 3$.

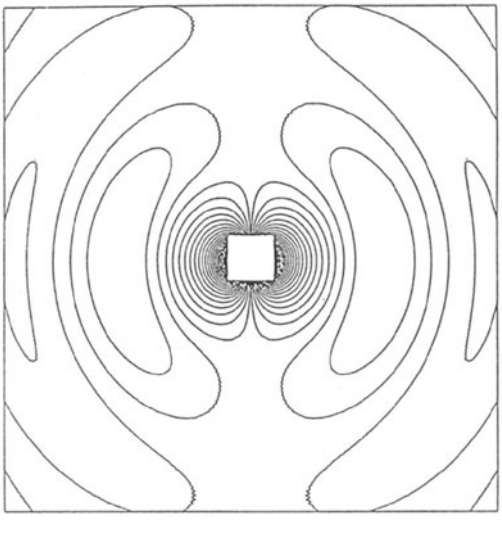

Figure 7. Contour plot in experiment III, without the composite material.

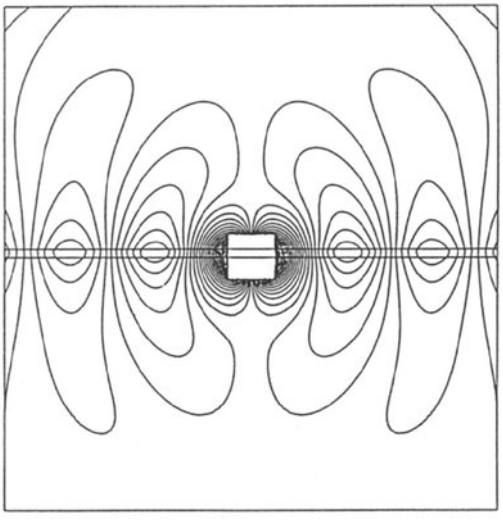

Figure 8. Contour plot in experiment III, $\epsilon_r = 6$.

REFERENCES

1 J. R. Wait and K. P. Spies, "Subsurface electromagnetic fields of a circular loop of current located above ground," IEEE Trans. Antennas Propagat., vol. AP-20, pp. 520-522, July 1972.

2 C. C. Lin and K. K. Mei, "Time Domain Absorbing Boundary Condition in Lossy Media," presented at Int. IEEE/Antennas Propagat. Soc. Symp., Boston, MA, June 1984.

3 R. F. Harrington, Time-Harmonic Electromagnetic Fields, McGraw-Hill Book Company, 1961.

4 M. E. Lee, S. I. Hariharan, and N. Ida, "Solving time-dependent two-dimensional eddy current problems," NASA Technical Memorandum, 100875 ICOMP-88-10, Lewis Research Center, Cleveland, OH, June 1988.

5 M. E. Lee, "Potential finite-difference time-domain methods for electromagnetic interface problems", Ph. D. dissertation, Dept. of Elec. Eng. , U. of Akron, Akron, OH, May 1989.